COBEM 2021 26th International Congress of Mechanical Engineering
November 22-26, 2021, Virtual Congress, Brazil

# COB-2021-0818
# AERODYNAMIC HEATING OF AN HYPERSONIC AIRBREATHING VEHICLE AT MACH NUMBER 5.8

**Paulo César de Oliveira Júnior**
**George Santos Marinho**
**Paulo Gilberto de Paula Toro**
**João Carlos Arantes Costa Júnior**
Universidade Federal do Rio Grande do Norte – Campus Universitário Lagoa Nova CEP 59078-970 Natal, RN - Brasil
paaulocz@gmail.com, gmarinho@ct.ufrn.br, toro11pt@gmail.com, arantes_jr@yahoo.com.br

***Abstract***. *In the aerospace sector there is a major limitation related to the payload that can be launched into orbit or beyond, due to the weight of the propulsion systems with chemical combustion, which are on board, currently used. In this context, several important studies carried out in the area of hypersonic propulsion, focusing on scramjet engines, which allow a greater payload because they do not need the oxidizer on board. Aerospace vehicles that use the hypersonic airbreathing propulsion system must include the conditions of hypersonic flight, resulting from aerodynamic and thermal loads. The hypersonic flight introduces extreme thermal loads at the vehicle's leading edges, resulting in high temperature around the surface; this effect is due to the transformation of the kinetic energy of the flow into thermal energy, producing a phenomenon called aerodynamic heating. Understanding this phenomenon is of paramount importance for determining the material to be used in the coating of the hypersonic aerospace vehicle, ensuring thermal protection to maintain the temperature of its internal walls at acceptable levels, as well as avoiding telemetry problems. Thus, the present work has as main objective to estimate the levels of heat flux (aerodynamic heating) to which the scramjet technological demonstrator will be subjected during an atmospheric flight at an altitude of 23 km and with a speed of 1723 m/s, corresponding to the number of Mach 5.8. Fay and Riddell, Lees, and Eckert methods are applied at the stagnation point, stagnation region, and at flat plate segments, respectively, for determining aerodynamic heating the at the aerospace vehicle integrated with a scramjet. The heat flux at the stagnation point is 2,558,209.22 W/m² and corresponds to the highest value found for the scramjet. At the intersection of the cylinder section and the deflection of the first ramp, a heat flux of 166,435.60 W/m² was verified, demonstrating the efficiency of the blunted region in reducing aerodynamic heating. In the ramps there is an increase in heat flux, but these values are significantly lower than the stagnation point and decrease along the flat region.*

***Keywords***: *aerospace vehicle, scramjet, heat flux, hypersonics.*

## 1. INTRODUCTION

On October 14, 1947, the experimental aircraft, sponsored by the U. S. government, named Bell XS-1, became the first manned supersonic aircraft to exceed the speed of sound in controlled level flight, by the Air Force test pilot Capt. Chuck Yeager. The Bell XS-1 research aircraft was installed in the bomb bay of the Boeing B-29, and the B-29 climbs to an altitude of approximately 20,000 feet (6,096 meters), and the XS-1 was drooped free from B-29 bomb bay. The rocket-powered Bell XS-1 research vehicle was fired by the veteran P-1 pilot Capt. Yeager, accelerating and climbing at the altitude of 43,000 ft (13,106.4 m), reaching 700 miles/h (312.928 m/s), corresponding to Mach number 1.06. At this supersonic velocity a strong bow shock wave was established in the air ahead of the XS-1 nose (Anderson, 2003).

On June 13, 1961, the experimental hypersonic rocket-powered X-15 airplane became the first manned hypersonic aircraft, to exceed five times the speed of sound, reaching a maximum velocity of 3,603 mph (1,610.685 m/s), corresponding to Mach number 5.3 (at about 32,500 meters geometric altitude), under control of the U.S. Air Force test pilot Major Robert White (Anderson, 2006). Both research vehicles, XS-1 and X-15, performed supersonic and hypersonic velocities into Earth dense atmosphere.

On April 12 and May 5, 1961, Russian Major Yuri Gagarin (U.S.S.R.) and North-American Alan Shepard (U.S.), respectively, using a multistage space rocket, became the first human beings to reach suborbital hypersonic flight. Alan Shepard's hypersonic flight reached an altitude of 115.7 miles (186,201.1 meters), entering the atmosphere at a speed above Mach number 5. Both Gagarin and Shepard Astronauts reached escape velocity, flew in space, orbiting the Earth, and safely return (Anderson, 2006).

Basically, aerospace vehicles, with sharp leading edges, as the research vehicles XS-1 and X-15, have been traveling in supersonic and hypersonic velocities flying into the dense atmosphere, inducing minimum drag, requiring lower thrust during ascent flight, but supporting severe aerothermodynamic loads. While, multistage space rocket reentry,

with high drag blunted shapes, minimizing the aerodynamic heating during the atmospheric reentry, as the U.S. Project Apollo and the Space Shuttle, have been traveling hypersonically from the Earth's upper atmosphere, decelerating from the orbit (Allen, 1958).

In this period, 1950-1960, several aerodynamic heating approaches were developed to be applied in the U.S. Projects Mercury Gemini and Apollo, primarily. The pioneer's Lees (1956) and Fay and Riddell (1958) theories provided the basic physical and mathematical understanding and modeling for convective aerothermodynamic fluxes for blunted aerospace vehicles flying in hypersonic velocities. At same period, Eckert (1955) and van Driest (1956) developed the engineering approaches applied to the plane surface.

The lessons learned from aerodynamic, and structural and thermal analysis was applied to the U.S. Space Shuttle. From that era (1960-1970), experimental (hypersonic) facilities (pulsed hypersonic tunnels) and Computation Fluid Dynamics (CFD) became mature technologies to be applied to aerospace vehicle design, including the U.S. Space Shuttle.

Simultaneously to the Project U.S. Space Shuttle (rocket-powered), several hypersonic programs were created to develop research aerospace vehicles using advanced airbreathing propulsion systems based on supersonic combustion (scramjet) technology. The most ambitious program was the National Aero-Space Plane (NASP), created in 1986, designed to be powered by a Single-Stage-To-Orbit (SSTO) reusable multi-cycle propulsion system and envisioned to take off horizontally from a conventional runway, using airbreathing propulsion to accelerate to hypersonic speeds, fly into space to achieve low Earth orbit, and return for a runway landing. In 1993, the NASP consortium carried out an analysis of cost reduction and, mainly, of the technical risks (too many immature technologies) resulting in the termination of the NASP program in 1995. However, the enormous amount of research, in ramjet (subsonic ramjet) and scramjet (supersonic combustion ramjet) technologies, created conditions to start a project less ambitious, Hyper-X, with the design of a technology demonstrator, called X-43 (Hallion, 1987).

In the aerospace sector there is a major limitation related to the payload that can be launched into orbit or beyond, due to the weight of the propulsion systems with chemical combustion, which are on board, currently used. In this context, several important studies carried out in the area of hypersonic propulsion, focusing on supersonic combustion (scramjet), which allows a greater payload because they do not need the oxidizer on board.

The lessons learned from the Space Shuttle reentry and the research developed over hypersonic airbreathing propulsion systems were applied to supersonic combustion (scramjet) technologies, including efficient aero-thermal-structural technologies to ensure adequate vehicle performance, increasing confidence of a successful flight, thereby mitigating risks during the flight testing of hypersonic vehicles.

In particular, the aerodynamic heating theories (Eckert, 1955; van Driest, 1956; Lees, 1956; Fay and Riddell, 1958), developed during 1950-1970, are applied, even today, to estimate, analytically, the convective flux over airbreathing vehicles flying in hypersonic velocities (Odam et al., 2005; Scigliano et al., 2016). Today, several research centers, including universities, have been developed in-house numerical codes to solve the aero-thermal-structure design of advanced hypersonic airbreathing vehicles, based on supersonic combustion (scramjet) (Cookrell et al., 2002; Di Benedetto et al., 2017; Scigliano et al., 2016; Favaloro et al., 2018). The aerodynamic heating based on experimental data obtained from hypersonic facilities (hypersonic shock tunnels) uses the engineering approaches, similar to the Eckert (1955), van Driest (1956), Lees (1956) and Fay and Riddell (1958).

Basically, aerodynamic heating, (heat flux) is proportional to cubed velocity and inversely proportional to the squared root of the radius (Fay and Riddell, 1958), thereby the aerodynamic heating increases the temperature of the structure rapidly, inducing high thermal stress, and changes the material properties. Hypersonic airbreathing vehicles, fly into the dense Earth atmosphere, for long time, then is exposed to a severe environment, can damage the airframe structure severely. It is essential to provide the vehicle temperature, in hypersonic velocities, accurately, to be possible to estimate the aerodynamic heating and predict the behavior of the structural materials and finally, to analyze the material structural deformation.

Generic scramjets in different flight conditions are under development by undergraduate and graduate engineering students from UFRN. The UFRN generic scramjet design to demonstrate the supersonic combustion technology at 30 km of altitude in hypersonic velocity of 2050 m/s (corresponding to Mach number 6.8), the thermodynamic airflow properties were determined, considering without and with boundary layer and calorically perfect gas (Toro et al., 2018a; 2018b, Carneiro, 2020, Carneiro et al., 2020). In these flight conditions, the aerodynamic heating was estimated, at the scramjet inlet leading-edge, blunted with a 1 mm radius, establishing a normal shock wave. Cold-wall heat flux was used, assuming the wall temperature remained constant at 300 K, and Fay and Riddell (1958), with Lewis number of one, and Lees (1956) theories were applied to the stagnation point and the cylinder section of the blunt-body geometry, respectively (Toro et al., 2018c).

Applying the same analytical-theoretical analysis, oblique shock wave, one-dimensional (Rayleigh) flow with heat addition, and Prandtl-Meyer expansion wave coupled to the area ratio, were applied to design the academic symmetrical plane scramjet flying at 1711 m/s (corresponding to Mach number 5.8) at 20 km of geometric altitude, to demonstrate the supersonic combustion of air/hydrogen mixture, at the combustion chamber (Fernandes Filho et al., 2020; Carvalho et al. 2020). Also, numerical analysis, using ANSYS Fluent code, was performed considering no hydrogen-air combustion, and no viscous effects to evaluate the accuracy of analytical design (Carvalho et al. 2020).

The main objective, of this work, was to estimate the levels of aerodynamic heating to which the technological demonstrator of supersonic combustion will be subjected during an atmospheric flight at an altitude of 23 km and with a speed of 1723 m/s (corresponding to the Mach number of 5.8). Fay and Riddell (1958), Lees (1956) and Eckert (1955) engineering methods were applied at the stagnation point, stagnation region (from the stagnation point to the intersection station of the blunted body and the first ramp deflection angle), and at flat surface segments, respectively.

## 2. SCRAMJET AND CHARACTERISTICS

Scramjet is the acronym of supersonic combustion ramjet, where the airflow, from the leading-to-trailing edges of the aerospace vehicle, remains supersonics, or greater than the speed of sound for a given static local temperature. The supersonic combustion process occurs at the combustion chamber of the aerospace vehicle flying, in velocities higher than five times the local sound speed, into the dense atmosphere, where there is enough atmospheric air (up to about 60 km-70 km of geometric altitude), to be captured during the fly of the aerospace vehicle. The airflow is compressed and decelerated, due to the oblique shock waves established at the compression section, to the adequate airflow temperature (higher than the fuel ignition temperature) and supersonic velocity (Mach number) at the entrance of the combustion chamber. The temperature and supersonic velocity airflow enable the mixture of the fuel and air, and the fuel (hydrogen)-air spontaneous combustion inside the combustion chamber, in supersonic velocities, producing sufficiently thrust for the aerospace vehicle to keep flying into the Earth atmosphere.

Due to the high-temperature environment of the hypersonic airflow; the total temperature, or enthalpy, is a function of the velocity squared power; the scramjet vehicles must have no moving parts. Therefore, the scramjet inlet geometry has to pressurize and decelerate the airflow, to the adequate conditions at the scramjet combustion chamber entrance capable to burn with the fuel at supersonic velocity. Also, the shock waves established in the scramjet inlet section must provide supersonic speeds at the entrance of the combustion chamber (Heiser and Pratt, 1994). Then, scramjet is a highly integrated system, where the hypersonic airbreathing propulsion system and vehicle are indistinguishable. Therefore, scramjets are unable to produce thrust while stationary. Consequently, another propulsion system has to accelerate the scramjet to supersonic combustion operation, at the combustion chamber, at flight conditions. Rocket engines may provide an affordable path for maturing hypersonic airbreathing components and subsystems in flight, and accelerate the scramjet to speed conditions, such that the shock waves established at the scramjet inlet be able to compress the atmospheric air achieving the operational conditions (Hass et al., 2005).

To better understand the features of the scramjet design, conventional terminology may be used. The scramjet operates according to (opened) Brayton thermodynamic cycle (Fig. 1) and may be divided into three main components (Fig. 2): external and internal compression section (inlet), combustion chamber (combustor), and internal and external expansion section (outlet) (Heiser and Pratt, 1994). The plane symmetrical scramjet (Fig. 2) consists of a two-wedge-derived waverider, symmetrical by a plane that passes through the leading-to-trailing edges, which each symmetrical part is a wedge-derived waverider.

Stations 0 and 1 are the scramjet and the cowl leading-edges, respectively (Fig. 2). Stations 3 and 4 are the entrance and exit of the combustion chamber, respectively (Fig. 2). Fuel is injected between the stations 3 and 4 (Fig. 2), at constant pressure (Fig. 1). Stations 9 and 10 are the cowl and the scramjet trailing-edges, respectively (Fig. 2). The combustion products are expanded directly into the Earth's atmosphere at atmospheric pressure at a given flight altitude, station 10 (Fig. 1), defining the opened thermodynamic process (Heiser and Pratt, 1994).

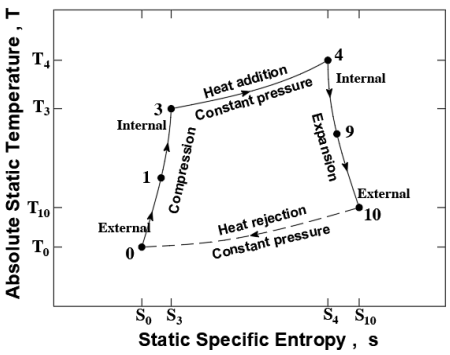


Figure 1. Brayton thermodynamic cycle of scramjet vehicles, adapted from Heiser and Pratt (1994).

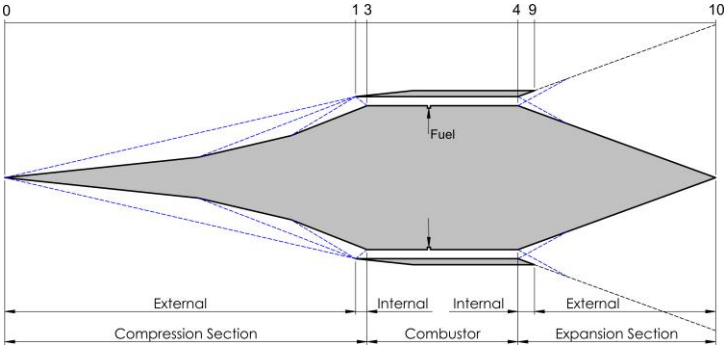


Figure 2. Plane symmetrical scramjet components and terminology, adapted from Heiser and Pratt (1994).

Basically, the mixed external and internal compression system, which is characterized by all incident oblique shock waves converge to the cowl leading-edge (shock on-lip), and the only one reflected shock wave converges to the combustion chamber entrance (shock on-corner) (Fig. 2). The external, stations 0 to 1, and internal, stations 1 to 3 (Fig.

2), at the adiabatic compression (inlet) section (Fig. 1) are governing by the incident and reflected oblique shock waves (Fig. 3). The combustion chamber section may be divided by constant area and constant pressure isolator, from the entrance, station 3, to fuel injection, and constant pressure supersonic combustion, from fuel injection to exit, station 4 (Fig. 1). The isolator is used to uniformize the flow from the compression section, and, in general, fuel is injected right after the isolator. The burning of hydrogen with the supersonic airflow at the combustion chamber is analytically simulated by the one-dimensional (Rayleigh) flow with heat addition (Fig. 3). The internal, stations 4 to 9, and external, stations 9 to 10 (Fig. 2), adiabatic expansion (outlet) section (Fig. 1) are governing by expansion wave (Prandtl-Meyer) flow coupled to area ratio (Fig. 3) (Anderson, 2003). The combustion products are expanded directly into the Earth's atmosphere at atmospheric pressure at a given flight altitude, station 10 (Fig. 2), opened thermodynamic process (Fig. 1) (Heiser and Pratt, 1994).

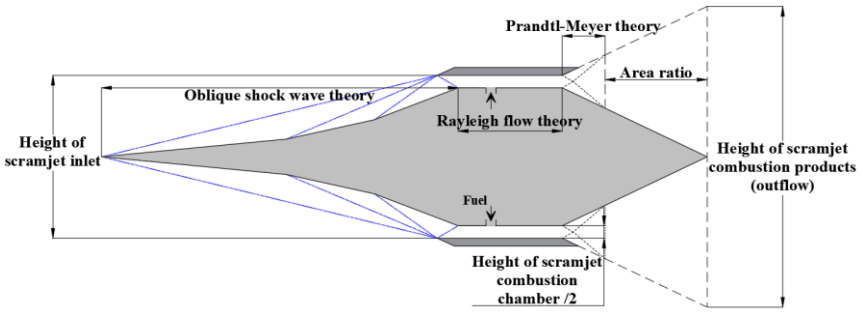


Figure 3. Two-Dimensional generic scramjet and analytical theories used (Carneiro, 2020).

As mentioned earlier, an important feature of the scramjet (Fig. 4) is a highly integrated system, where the propulsion system and vehicle are indistinguishable. This tight integration is caused by the fact that the frontal (compression) section of the vehicle contributes to the compression of atmospheric air, while the rear (expansion) section contributes to the generation of thrust (Figs. 2 to 3). The net thrust produced by the scramjet is the difference between the thrust (the force that propels the vehicle), generated by the expansion of exhaust gases from the rear of the scramjet, and the total drag (the force that resists the movement of the vehicle). These forces may produce thrust to the scramjet flight or not depending on the balance of these forces in scramjet vehicle design.

From the lessons learned from U.S. Apollo and U.S. Space Shuttle designs, the hypersonic airbreathing vehicle design must fly at the constant dynamic pressure trajectory. Flying at higher dynamic pressure than 96,000 Pa means the scramjet will be too heavy, required larger structural material thickness, for sustained atmosphere flight, while, for lower dynamic pressure than 23,000 Pa, the scramjet will need a large wing area. Also, to generate adequate thrust to reach and sustain high speed flight, the hypersonic airbreathing (scramjet) vehicles must fly at Earth's dense atmosphere to capture and process the surrounding atmosphere air. The constant dynamic pressure trajectory and the freestream mass airflow per unit area (Fig. 5) are the corridor that any aerospace vehicle using airbreathing propulsion must obey, including the hypersonic airbreathing propulsion based on supersonic combustion (Heiser and Pratt, 1994).

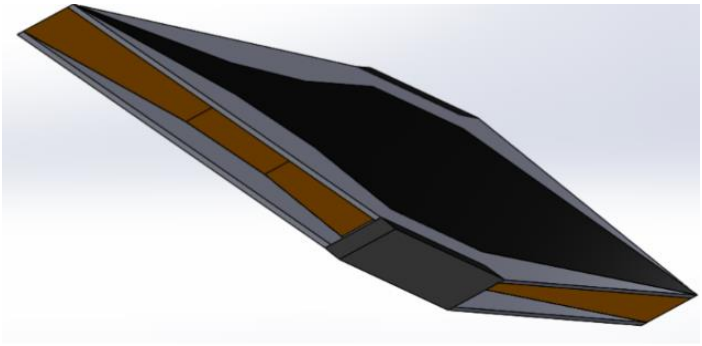

Figure 4. Generic supersonic combustion (scramjet) demonstrator (Carneiro, 2020).

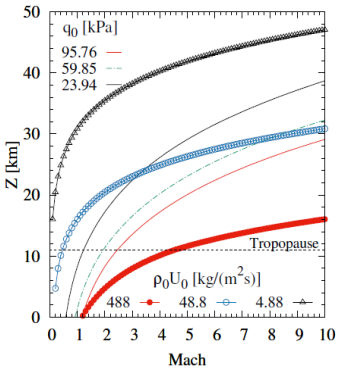


Figure 5. Constant dynamic pressure and freestream mass airflow per unit area (Araujo et al., 2021).

## 3. METHODOLOGY

As mentioned earlier, to minimize the aerodynamic heating, any aerospace vehicle, flying into dense atmosphere, must be blunted (Allen, 1958), and the aerodynamic heating, at the stagnation point of blunted vehicle, is inversely

proportional to the squared root of the radius (Fay and Riddell, 1958). On top of that, due to extremely difficult to manufacture a sharp leading-edge, it was recommended, from NASP design, a scramjet leading-edge with very low radius, at least 0.1-in (2.54 mm) (Albertson and Venkat, 2005).

Although Computational Fluid Dynamics (CFD) simulations are used to validate a scramjet design prior to expensive flight testing, these computationally expensive analysis is prohibitive at the preliminary design, where numerous design iterations are commonly necessary. Analytical theory to estimate the aerodynamic heating is essential to provide the boundary conditions for thermal analysis.

### 3.1 Aerodynamic heating applied to the scramjet compression section

The heat flux along the aerodynamic surface of the scramjet was determined using Fay and Riddell (1958), Lees (1956) and Eckert (1955) methods.

#### 3.1.1 Aerodynamic heating at blunted stagnation point

Fay and Riddell (1958) presented the theory of stagnation point heat transfer in dissociation air, considering Prandtl number Pr 0.71, and for spherical blunted nose (Fig. 6), given by

$$\dot{q}_o = \frac{0.763}{(\mathrm{Pr})^{0.6}} (\rho_s \mu_s)^{0.4} (\rho_w \mu_w)^{0.1} (H_s - h_w) \left[ 1 + \left( Le^{0.52} - 1 \right) \frac{h_d}{H_s} \right] \left[ \left( \frac{du_e}{dx} \right)_{t2} \right]^{0.5} \tag{1}$$

$$\left( \frac{du_e}{dx} \right)_s = \frac{1}{R} \sqrt{\frac{2(p_s - p_\infty)}{\rho_s}} \tag{2}$$

where: $p$, $\rho$, $\mu$, $h$, $R$, and $\left( \frac{du_e}{dx} \right)_s$, are pressure, density, dynamic viscosity, enthalpy, radius and airflow velocity gradient, respectively. The subscribers $\infty$, $s$, $w$, and are the properties of the flight conditions (freestream atmospheric air), right after the normal shock wave established ahead of the blunted cylindrical nose (neglecting the isentropic airflow from after normal shock to the stagnation point and in the wall, respectively. Assuming Lewis number unity, the $\rho\ \mu$ variation effect is very close to that found for the equilibrium boundary layer.

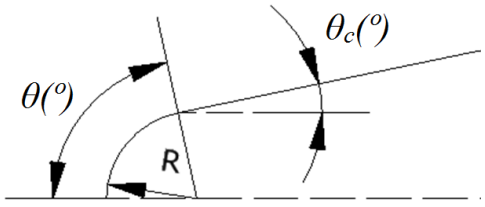


Figure 6. Blunted region and first scramjet compression ramp (Lara et al., 2018).

Considering the cylindrical blunted nose, van Driest (1956) recommended replace 0.763 by 0.570, and considering the conservation energy, in enthalpy (for real gas effects) or in temperature (assuming calorically perfect gas) forms, respectively; thereby, for heat transfer at cylindrical stagnation point, and Lewis number unity, is given by

$$\dot{q}_o = \frac{0.570}{(\mathrm{Pr})^{0.6}} (\rho_s \mu_s)^{0.4} (\rho_w \mu_w)^{0.1} (H_s - h_w) \left[ \left( \frac{du_e}{dx} \right)_{t2} \right]^{0.5} \tag{3}$$

$$h_o = h + \frac{u^2}{2} \tag{4}$$

$$\frac{T_o}{T} = 1 + \frac{\gamma - 1}{2} M^2 \tag{5}$$

First, the blunted scramjet leading-edge conditions may be treated as those behind a normal shock wave. Unfortunately, the unsteady heat-transfer rate is very difficult to estimate, because should be estimated during the aerospace vehicle atmospheric flight. Therefore cold-wall heat-transfer rates were estimated by assuming the wall temperature remained constant at 300 K. Finally, the external airflow properties are much more important than the cold-wall values in estimate the heat-transfer rate, and the heat-transfer rate is inversely proportional to blunted leading-edge cylindrical nose.

### 3.1.2 Aerodynamic heating on blunted region

Lees (1956) presented theory of laminar heat transfer over blunt-nosed bodies at hypersonic flight speeds (high stagnation temperatures), in dimensionless enthalpy gradient at the surface, represented very accurately by the classical zero pressure gradient value, and the surface heat-transfer rate distribution is obtained directly in terms of the surface pressure distribution (Fig. 6). This method was applied, in the present work, to the blunted cone capped by a cylindrical segment.

$$\frac{\dot{q}_w}{\dot{q}_o} = \frac{2\theta \sin\theta \left\{ \left[ 1 - \frac{1}{\gamma M_\infty^2} \right] \cos^2\theta + \frac{1}{\gamma M_\infty^2} \right\}}{[D(\theta)]^{0.5}} \tag{6}$$

$$D(\theta) = \left[ 1 - \frac{1}{\gamma M_\infty^2} \right] \left[ \theta^2 - \frac{\theta \sin 4\theta}{2} + \frac{1 - \cos 4\theta}{8} \right] + \frac{4}{\gamma M_\infty^2} \left[ \theta^2 - \theta \sin 2\theta + \frac{1 - \cos 2\theta}{2} \right] \tag{7}$$

where: $\infty$ is the flight velocity, and the dimensionless heat-transfer is function on geometry position $\theta$, and the stagnation heat-transfer is given by the at blunted stagnation point (Fay and Riddell, 1958).

### 3.1.3 Aerodynamic heating on plane surface

Eckert (1955) presented the engineering relations for heat transfer to surfaces in high velocity flow (Fig. 6). Considering no high temperature effects and air behavior as calorically perfect gas, the heat transfer rate is given by:

$$\dot{q}_w = S_t^* \rho^* u_e c_p \left( T_r - T_w \right) \tag{8}$$

$$T_r = \left( 1 + r \frac{\gamma - 1}{2} M_e^2 \right) T_e \tag{9}$$

$$S_t^* = \frac{0.332}{\sqrt[3]{Pr^*} \sqrt{Re_x^*}} \tag{10}$$

$$Re_x^* = \frac{\rho^* u_e x}{\mu^*} \tag{11}$$

$$T^* = T_e + 0.5 \left( T_w - T_e \right) + 0.22 \left( T_r - T_e \right) \tag{12}$$

where: $S_t^*$ and $\rho^*$ means Stanton number and density respectively. Both, should be estimated by reference temperature $T^*$. $u_e$ and $c_p$ are the airflow velocity external of the boundary layer, and the specific heat at constant pressure, respectively. $T_r$ and $T_w$ are the recovery temperature and wall temperature, respectively.

### 3.2 Aerodynamic relations applied to the scramjet compression section

In the analytical theoretical analysis, the subscripts *in* and *out* are used to identify the upstream (inlet) and the downstream (outlet) conditions, respectively, of each station (Fig. 6) of the generic scramjet inlet baseline.

#### 3.2.1 Normal shock wave (at the stagnation point)

Applying the mass, momentum and energy conservation laws for a compressible gas, considering the hypotheses of one-dimensional, uniform, isentropic, stationary and calorically perfect flow, the normal shock relationship can be obtained as a function of the upstream Mach number (Anderson, 2003), given by:

$$\frac{p_{out}}{p_{in}} = 1 + \frac{2\gamma}{(\gamma+1)}\left(M_{in}^2 - 1\right) \tag{13}$$

$$\frac{\rho_{out}}{\rho_{in}} = \frac{u_{in}}{u_{out}} = \frac{(\gamma+1)M_{in}^2}{\left[(\gamma-1)M_{in}^2 + 2\right]} \tag{14}$$

$$\frac{T_{out}}{T_{in}} = \frac{\frac{p_{out}}{p_{in}}}{\frac{\rho_{out}}{\rho_{in}}} \tag{15}$$

$$M_{out} = \sqrt{\frac{M_{in}^2 + \frac{2}{(\gamma-1)}}{\frac{2\gamma}{(\gamma-1)}\ M_{in}^2 - 1}} \tag{16}$$

#### 3.2.2 Oblique shock wave

Applying the mass, momentum and energy conservation laws, considering two-dimensional steady state, compressible flow, non-viscous effects, no heat conduction, and for calorically and/or thermally perfect gas ( $p = \rho RT$, $\gamma = \text{constar}$) the oblique shock relationships (Fig. 3) can be easily obtained as closed form of the shock wave angle $\beta$, Mach number across the oblique shock wave, and the thermodynamic property (static pressure, static density and static temperature) ratios (Anderson, 2003), given by:

$$tg\theta_s = 2(\text{cotg}\beta)\left[\frac{\left(M_{in}\ sen\beta\right)^2 - 1}{M_{in}^2(\gamma + \cos 2\beta) + 2}\right] \tag{17}$$

$$M_{out} = \left[\frac{1}{sen\left(\beta - \theta_s\right)}\right]\sqrt{\frac{\left(M_{in}\, sen\beta\right)^2 + \frac{2}{(\gamma-1)}}{\frac{2\gamma}{(\gamma-1)}\ \left(M_{in}\, sen\beta\right)^2 - 1}} \tag{18}$$

$$\frac{p_{out}}{p_{in}} = 1 + \frac{2\gamma}{(\gamma+1)}\left[\left(M_{in}\ sen\beta\right)^2 - 1\right] \tag{19}$$

$$\frac{\rho_{out}}{\rho_{in}} = \frac{(\gamma+1)\left(M_{in}\ sen\beta\right)^2}{\left[(\gamma-1)\left(M_{in}\ sen\beta\right)^2 + 2\right]} \tag{20}$$

$$\frac{T_{out}}{T_{in}} = \frac{\frac{p_{out}}{p_{in}}}{\frac{\rho_{out}}{\rho_{in}}} \tag{21}$$

where: $\rho$, $p$, $T$ are density, pressure, and temperature of the gas, respectively, function of the incoming local supersonic/hypersonic flow Mach number $M_{in}$, the gas from the atmosphere $\gamma$ (air in the Earth's planet, $\gamma = 1.4$) and the oblique shock wave $\beta$. For a given deflection (turning) angle $\theta_s$ the oblique shock wave $\beta$ may be obtained iteratively with the relationship $\theta - \beta - M$. Note, the flow across the oblique shock wave promote an increase of pressure, density, temperature, and a decrease of Mach number, however the flow remains supersonic/hypersonic and parallel to the flat surface of the external compression section (Fig. 3).

## 4. RESULTS AND COMMENTARIES

The UFRN scramjet was designed to fly from (geometric) altitude of 23 km, with hypersonic velocities of 1723 m/s. Therefore, it is necessary to define the thermodynamic atmospheric air properties for this condition (Tab. 1).

Table 1. Thermodynamic atmospheric properties at 23 km geometric altitude.

| Thermodynamic atmospheric properties (U.S. Standard Atmosphere, 1976) | | | | | Flight conditions | |
|---|---|---|---|---|---|---|
| Altitude km | Temperature K | Pressure Pa | Density kg/m$^3$ | Sound speed m/s | Velocity m/s | Mach number |
| 23 | 219.57 | 3466.86 | 0.05501 | 297.05 | 1723 | 5.80 |

### 4.1 Normal shock

The thermodynamic properties after a normal shock wave (Tab. 2) were determined by Eqs. 13-16. As shown in Table 1, atmospheric flight at a geometric altitude of 23 km and a speed of 1723 m/s was considered.

Table 2. Thermodynamic properties at the generic scramjet, altitude 23 km, flight velocity 1723 m/s.

| | | Station 0 | Across normal shock |
|---|---|---|---|
| $M_{in}$ | - | 5.80 | 5.80 |
| $M_{out}$ | - | - | 0.41 |
| $p_{out}/p_{in}$ | - | - | 39.09 |
| $T_{out}/T_{in}$ | - | - | 7.48 |
| $\rho_{out}/\rho_{in}$ | - | - | 5.22 |
| p | Pa | 3,466.86 | 135,502.70 |
| T | K | 219.57 | 1,642.86 |
| ρ | kg/m$^3$ | 0.05501 | 0.28733 |
| a | m/s | 297.04 | 812.54 |
| u | m/s | 1,723.00 | 329.84 |
| $T_{total}$ | K | 1,697.08 | 1,697.01 |

### 4.2 Oblique shock

In flight condition (Tab. 1) the scramjet was designed with three compression ramps, with the turning (deflection) angles (Tab. 3) considering maximum total pressure recovery and all incident shock waves are of equal strength, where in each case, the shock on-lip (all incident shock converged to the cowl leading-edge) and shock on-corner (the only reflected shock converged to combustion chamber entrance) conditions were guaranteed (Figs. 2 and 3), satisfying the combustion chamber entrance conditions of $T_3$ of about 1024.95 K and $M_3$ of 1.81.

Table 3. Deflection angles and combustion chamber entrance conditions for scramjet at 23 km altitude.

| | $\theta_1$ | $\theta_2$ | $\theta_3$ | $T_3$ | $M_3$ |
|---|---|---|---|---|---|
| 23 (km) / speed 1723 m/s (Mach 5.8) | 7.25º | 8.60º | 10.30º | 1024.95 | 1.81 |

The $\theta - \beta - M$ relation was applied to obtain the incident oblique shockwave angles as well as the reflected oblique shockwave angle. Following, the thermodynamic air properties after each event may be evaluated by the thermodynamic property ratio and the freestream thermodynamic properties (Tab. 1). The Mach number after each incident and reflected shock wave may be evaluated by Eqs. 17-21 (Tab. 4).

For no hydrogen-air combustion, the generic scramjet, with three ramps at the compression section (Figs. 2-3), with leading-edge angle of 7.25º, followed by two deflection angles of 8.6º and 10.3º, flying at 23 km of geometric altitude with speed 1723 m/s corresponding at Mach number 5.8 is capable to generate a supersonic velocity corresponding to Mach number of 1.81 and a static temperature of 1024.95 K, higher than 845.15 K, ignition temperature of hydrogen, at the entrance of combustion chamber. Consequently, it is possible to demonstrate a supersonic combustion when hydrogen may burn the supersonic atmospheric air, at the combustion chamber, during the atmospheric hypersonic flight of this generic scramjet.

Table 4. Thermodynamic properties at the generic scramjet, altitude 23 km, flight velocity 1723 m/s.

| | | Station 0 | 1st ramp | 2nd ramp | 3rd ramp | Reflection | Entrance |
|---|---|---|---|---|---|---|---|
| $M_{in}$ | - | 5.80 | 5.80 | 4.87 | 4.04 | 3.30 | 1.81 |
| $\theta$ | º | - | 7.25 | 8.60 | 10.30 | 26.15 | - |
| $\beta$ | º | - | 15.37 | 18.40 | 22.35 | 43.45 | - |
| $M_{in}sen\beta$ | - | - | 1.54 | 1.54 | 1.54 | 2.27 | - |
| $M_{out}$ | - | - | 4.87 | 4.04 | 3.30 | 1.81 | 1.81 |
| $p_{out}/p_{in}$ | - | - | 2.59 | 2.59 | 2.59 | 5.83 | - |
| $T_{out}/T_{in}$ | - | - | 1.35 | 1.35 | 1.35 | 1.92 | - |
| $\rho_{out}/\rho_{in}$ | - | - | 1.93 | 1.93 | 1.93 | 3.04 | - |
| p | Pa | 3,466.86 | 8,985.24 | 23,279.09 | 60,324.86 | 351,741.24 | 351,741.24 |
| T | K | 219.57 | 295.41 | 397.41 | 534.66 | 1,024.95 | 1024.95 |
| $\rho$ | $kg/m^3$ | 0.05501 | 0.10596 | 0.20406 | 0.39306 | 1.19553 | 1.19553 |
| a | m/s | 297.05 | 344.56 | 399.64 | 463.54 | 641.79 | 641.79 |
| u | m/s | 1,723.00 | 1,678.19 | 1,615.98 | 1,528.26 | 1,162.08 | 1,162.08 |
| $T_{total}$ | K | 1,697.01 | 1,697.01 | 1,697.01 | 1,697.01 | 1,697.01 | 1,697.01 |

Note, the supersonic airflow across the oblique attached (incident and reflected) shockwave promoted an increase of thermodynamic properties (pressure, temperature, density, and speed of sound) and a decrease of flow velocity (Mach number), and the streamline of the airflow remains supersonic and parallel to the flat surface (Tab. 4) of the generic scramjet compression section. Also, pressure ratio, temperature ratio, density ratio as well as the product $M_{in}$ sen$\beta$ are constant for all incident shock waves, characteristics of same shock strength. Finally, the total temperature from the leading-edge to combustion chamber entrance is constant. Therefore, the airflow velocity is slight lower than the flight scramjet condition, 23 km, 1723 m/s, and Mach number 5.8 (Tab. 3) and corresponding results (Tab. 4).

### 4.3 Aerodynamic heating

Applying the stagnation point heat transfer theory in the dissociation air (Fay and Riddell, 1958) and considering van Driest's (1956) recommendation for a cylindrical blunted nose (Eqs. 2-5), a stagnation point heat flux of 2,558,209.22 W/m² was determined, which corresponds to the highest value found for the scramjet. This is due to the deceleration caused by the normal shock wave, and then the isentropic deceleration to the stagnation point, which also results in an increase in thermodynamic properties (pressure, temperature, density and speed of sound).

The aerodynamic heating estimated by Lees (1956) theory (Eqs. 6 and 7) presents a sinusoidal behavior as expected (Fig. 7). The relation $q_w/q_o$=1 corresponding to the heat flux value at the stagnation point. The aerodynamic heating at the intersection of the cylinder section and the first ramp deflection of 7.25° is 166,435.60 W/m². Thus, the heat flux decreased 93.49%, demonstrating that the blunted region has a high efficiency in reducing the heat flux distribution value (Fig. 7).

The heat flux along the ramps of the scramjet inlet (Fig. 8) is calculated using the theory of Eckert (1955) (Eqs. 8-12), the intersection between the cylindrical section and the first ramp occurs at 0.02 m, being registered a heat flux of 83,317.30 W/m². There is a reduction in the heat flux along the first ramp of about 77.66%, in addition, in this region the flow is laminar. In the passage to the second ramp the flow becomes turbulent and there is a significant increase in the heat flux to 155,411.21 W/m², but along the ramp there is a reduction in the flow of about 6.81%. The flow remains turbulent for the third ramp, with another jump in the heat flux value, in this case to 335,357.81 W/m², however, a reduction of approximately 4.51% is recorded along this ramp.

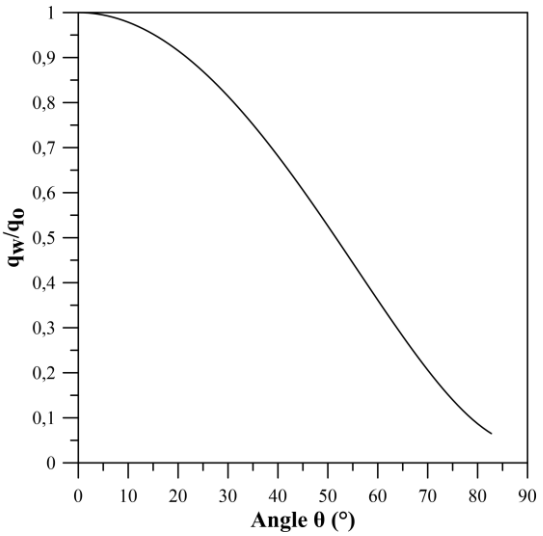


Figure 7. Heat flux along the angular distance around the blunt region of the scramjet.

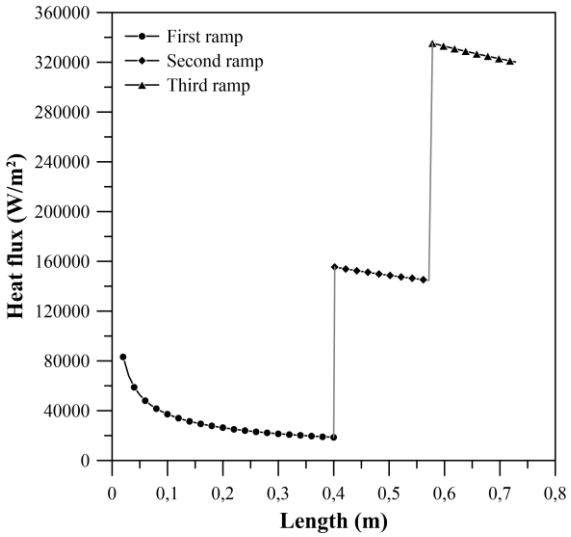


Figure 8. Heat flux along the ramps of the scramjet inlet.

## 5. CONCLUSIONS

To calculate the thermodynamic properties, the oblique shock wave theory was used, which govern the compression section of the scramjet. The generic scramjet, with three ramps in the compression section, with deflection angles of 7.25 °, 8.60 ° and 10.30 °, in the flight condition at an altitude of 23 km and speed of 1723 m/s, corresponding to Mach number 5.8, it is capable of generating, at the entrance of the combustion chamber, a flow with a speed of Mach 1.81 and a temperature above 845.15 K, showing a possibility of burning hydrogen spontaneously, ensuring self-ignition of the scramjet vehicle, as well as perform supersonic combustion.

To calculate the heat fluxes, Fay and Riddell theories (stagnation point), Less theory (blunted region) and Eckert theory (ramps of the scramjet inlet) were used. The highest value for the heat flux was verified at the stagnation point, this is due to the subsonic deceleration caused by the normal shock wave and later by the isentropic deceleration to the stagnation point. These decelerations also contribute to the increase in thermodynamic properties (pressure, temperature, density and speed of sound). However, the blunted region allowed a reduction of 93.49% of this, contributing to the heat flow to reach flat regions with less drastic values. Still, the sinusoidal behavior of the heat flux in the blunted region is in agreement with what was verified and presented by Lees. For the first ramp it was verified laminar flow and for the second and third ramp turbulent flow. As there is an increase in thermodynamic properties in each of these, there is also an increase in the heat flux, but at values much lower than that determined for the stagnation point.

## 6. ACKNOWLEDGEMENTS

This study was financed in part by the Coordenação de Aperfeiçoamento de Pessoal de Nível Superior - Brasil (CAPES) - Finance Code 001. Also, the authors would like to thank CAPES the support given by the Project PROCAD-DEFESA 88887.626266/2021-00. The authors would like to thank Universidade Federal do Rio Grande do Norte (UFRN) to support granted to carry out research on hypersonic airbreathing propulsion.

## 7. REFERENCES

Albertson, C., & Venkat, V. (2005). Shock Interaction Control for Scramjet Cowl Leading Edges. AIAA/CIRA 13th International Space Planes and Hypersonics Systems and Technologies Conference. doi:10.2514/6.2005-3289

Allen, H. J. (1958). Hypersonic Flight and the Re-Entry Problem: The Twenty-First Wright Brothers Lecture. Journal of the Aerospace Sciences, 25(4), 217–227. doi:10.2514/8.7600

Anderson Jr., J. D. (2003). Modern Compressible Flow: with Historical Perspective. McGraw-Hill series in Aeronautical and Aerospace Enginnering. Third Edition. ISBN O-07-242443-5. ISBN 0-07-1 12161-7 (ISE).

Anderson Jr., J.D. (2006). Hypersonic and high temperature gas dynamics. Washington, DC: AIAA Education Series.

Araújo, P. P. B., Sabino Pereira, M. V., Marinho, G. S., Martos, J. F. A., Toro, P. G. P. (2021). Optimization of scramjet inlet based on temperature and Mach number of supersonic combustion. Aerospace Science and Technology.

Carneiro, R., Aráujo, P. P. B., Borba, G. L., Marinho, G. S., Toro, P. G. P. (2020). Influence of the boundary layer on the design of the compression section of a generic scramjet. 18th Brazilian Congress of Thermal Sciences and Engineering. (ENCIT 2020-0805). Online.

Carneiro, R. (2020). Estudo analítico de um demonstrador da tecnologia da combustão supersônica. Dissertação de Mestrado. Programa de Pós-Graduação em Engenharia Mecânica. UFRN.

Carvalho, L., A., S., Santos, L., M., C., Fernandes Filho, J., Araújo, P. P. B., Medeiros, J. B., Toro, P. G. P. (2020). Academic scramjet Design to flight at 20 km of altitude at Mach number 5.79 integrated at rocket engine S30. 18th Brazilian Congress of Thermal Sciences and Engineering. (ENCIT 2020-0547). Online.

Cockrell, C., Auslender, A., White, J., & Dilley, A. (2002). Aeroheating predictions for the X-43 hyper-X cowl-closed configuration at Mach 7 and 10. 40th AIAA Aerospace Sciences Meeting & Exhibit. doi:10.2514/6.2002-218

Di Benedetto, S.; Di Donato, M.P.; Rispoli, A.; Cardone, S.; Riehmer, J.; Steelant, J.; Vecchione, L. (2017). HEXAFLY-INT Project: Design of a High Speed Flight Experiment ESA; 2nd International Symposium on Hypersonic Flight: from 100.000 to 400.000ft, Location: Rome, Italy. Proceedings of ISHF

Eckert, E. R. G., "Engineering relations for friction and heat transfer to surfaces in high velocity flow," Journal of the Aeronautical Sciences, Vol. 22, No. 8, 1955, pp. 585–587.

Favaloro, N., Di Donato, M.P., Rispoli, A. et al. Preliminary Analysis of the Hexafly-International Vehicle. Aerotec. Missili Spaz. 97, 113–128 (2018). https://doi.org/10.1007/BF03404765

Fay, J. A. and Riddell, F. R. "Theory of stagnation point heat transfer in dissociated air". Journal of the Aeronautical Sciences, Vol. 25, No. 2, 1958, pp. 73–85.

Fernandes Filho, J., Carvalho, L., A., S., Santos, L., M., C., Marinho, G. S., Medeiros, J. B., Toro, P. G. P. (2020). Preliminary design and analysis of a generic scramjet air for atmospheric flight at Mach number 5.8. 18th Brazilian Congress of Thermal Sciences and Engineering. (ENCIT 2020-0649). Online.

Hallion, R. P. (1987). The Hypersonic Revolution, Vol. II: From Scramjet to the National Aero-Space Plane, 1964-1986, Aeronautical Systems Division, Wright-Patterson AFB, OH.

Hass, N., Smart, M., & Paull, A. (2005). Flight Data Analysis of the HyShot 2. AIAA/CIRA 13th International Space Planes and Hypersonics Systems and Technologies Conference. doi:10.2514/6.2005-3354

Heiser, W.; Pratt, D.; Daley, D.; Mehta, U. (1994). Hypersonic Airbreathing Propulsion. AIAA Education Series. ISBN 1-56347-035-7. https://doi.org/10.2514/4.470356

Lara, A. M. P., Toro, P. G. P., Rêgo, I. S., Rolim, T. C. (2018). Heat flux and thermodynamic properties analysis at the stagnation point and the blunt region of the 14-X S scramjet engine. ENCIT 2018-0462.

Lees, L. (1956). Laminar Heat Transfer Over Blunt-Nosed Bodies at Hypersonic Flight Speeds. Journal of Jet Propulsion, 26(4), 259–269. doi:10.2514/8.6977

Odam, J, Neely, A., Stewart, B., Boyce, R. (2005). Heating Analysis of a Generic Scramjet. AIAA/CIRA 13th International Space Planes and Hypersonics Systems and Technologies Conference., AIAA 2005-3338. Italy.

Scigliano, R., Pezzella, G., Marini, M., Di Benedetto, S., & Steelant, J. (2016). Aerothermal Design of the Hexafly-int Glider. AIAA SPACE 2016. doi:10.2514/6.2016-5627

Toro, P. G. P.; Carneiro, R.; Araújo, J. W. S.; Marinho, G. S.; Borba, G. L.; Rego, I. S.; Martos, J. F. A. (2018a). Design and Analysis of a generic scramjet air inlet. 17th Brazilian Congress of Thermal Sciences and Engineering (ENCIT 2018-0751). Águas de Lindóia/SP, Brazil.

Toro, P. G. P.; Carneiro, R.; Araújo, J. W. S.; Marinho, G. S.; Borba, G. L.; Rego, I. S.; Martos, J. F. A. (2018b). Design of the Generic Scramjet Combustion Chamber. 17th Brazilian Congress of Thermal Sciences and Engineering (ENCIT 2018-0056). Águas de Lindóia/SP, Brazil.

Toro, P. G. P.; Fernandes, A. G. L. N.; Marinho, G. S.; Borba, G. L.; Martos, J. F. A.; Rego, I. S. (2018c). A new approach to optimize the scramjet inlet design applying the total pressure recovery. 17th Brazilian Congress of Thermal Sciences and Engineering (ENCIT 2018-0074). Águas de Lindóia/SP, Brazil.

U.S. Standard Atmosphere. (1976). NASA TM-X 74335. National Oceanic and Atmospheric Administration, National Aeronautics and Space Administration and United States Air Force.

## 8. RESPONSIBILITY NOTICE

The Authors are the only responsible for the printed material included in this scientific article.
The Authors declare that there is no conflict of interest regarding the publication of this scientific article.